Journal of Computers Vol. 34 No. 1, February 2023, pp. 45-61
doi: 10.53106/199115992023023401004

Image Denoising Method Based on Harmonic Filtering and Non-Subsample Shear Wave Block Matching in Wavelength Domain

Chun-Yan Jiang[1*], Rong Gou[2], Feng Shi[1]

[1] School of Design, Jiangsu Open University, Nanjing 210000, China
wujingxyz123@163.com, 932759228@qq.com
[2] School of Information Technology, Jiangsu Open University, Nanjing 210000, China
124530790@qq.com

Received 7 April 2022; Revised 6 July 2022; Accepted 10 August 2022

Abstract. Efficient noise filtering is the difficulty of image denoising on the premise of preserving the edge and internal texture information of the image. Therefore, this paper focused on adaptive Gaussian variational model and block matching image denoising method in the wave domain from the non-local point of view. At first, a 3D block match harmonic filtering model was establish in that wavelet domain, 3D transform was use to represent that real signals in the match block group in a sparse form, then the shrinkage threshold was used to achieve the purpose of pre-denoising, and the wavelet transform was then used to extract the high frequency part of the predictor image for filtering. In order to avoid edge blurring, Laplace-Gaussian algorithm was used to construct a new operator into the diffusion model, and the wavelet coefficients were reconstructed to obtain the final approximation of the original image. Secondly, a block matching denoising model based on shear wave was proposed. In order to avoid ill-conditioned problem, The multi-scale geometric analysis method using shearlet transform can improve the edge protection ability, and a block matching denoising model based on shearlet is proposed. The new model predicts the scaling threshold according to the statistical characteristics of the histogram, performs hard threshold filtering on the high-frequency sub-band to obtain the processed sub-band coefficients, and performs block matching 3D filtering on the decomposed low-frequency sub-band coefficients to obtain the processed coefficients. All processed subband coefficients are inversely transformed and reconstructed to obtain a denoised image. The analysis and simulation results showed that the two new models can effectively suppress noise and improve the clarity, and the block matching denoising based on shear wave had more advantages.

Keywords: image denoising, wavelet transform, Laplace-Gaussian algorithm, block matching, shear wave transform

1 Introduction

With the increasing combination of computer vision and multimedia applications, image processing technology will be used in almost all areas of life. However, in the process of image acquisition, compression or transmission, noise is very easy to be introduced, which affects the subsequent work. Therefore, image denoising is particularly important in the process of image processing. At present, image processing methods mainly include two categories: spatial domain processing and transform domain processing. In the transform domain processing, it will be divided into frequency domain processing and wavelet domain processing.

Perona and Malik [1] proposed an adaptive diffusion (PM) model in 1990, and Rudin et al. [2] first proposed a total variation (TV) regularization model in 1992. Because the model does not completely conform to the morphological principles of image processing, there are likely to be step-like oscillations at the edges of images. In order to avoid this oscillation effect, Zhou Xianchun et al. proposed a fully variational coupled image denoising model [3], which uses the edge detection characteristics of Canny operator to design a control function, effectively suppressing the "stair-step effect" of TV model.

Yu et al. [4] introduced two new diffusion coefficients and a residual term, using the fractional differentiation operator in the PM model and introducing local variance to adaptively adjust the order of fractional differentiation. In 2021, Zhao et al. proposed an RFSB model based on the TV model [5]. The model first separates edges and smooth regions according to structural features, and uses the split-Bregman method and the region fusion

* Corresponding Author

method, to fuse the TV model and the TV least squares function model. Effective protection of edge information.

Donoho [6] has proved the feasibility of wavelet threshold denoising method in theory, and has greatly improved the effect of noise removal and edge structure protection. Since then, the relevant research based on wavelet theory has gradually become a hot topic in image denoising field [7-10]. In 2005, Buades proposed Non-Local Means (NLM) [11] filtering based on the properties of Gaussian white noise. This algorithm is simple to compute and has been studied deeply by many scholars [12-13]. In 2007, Dabov et al proposed a Block of 3Dimension (BM3D) [14] image denoising algorithm based on sparse representation, combining NLM method and wavelet transform method. Because of its outstanding effect, many scholars have studied and improved BM3D image denoising algorithm [15-17]. Denoising methods based on BM3D have been proposed one after another, but there is no good balance between noise removal and edge information protection. Guo et al. [18] propose that by use of a framework of affine systems with synthetic expansion. Although the Shearlet geometric transform denoising method based on multi-dimensional function sparse representation has a good sparse representation effect, it does not have the translational property because of the down-sampling operation, which makes the image prone to phase distortion in the denoising process and pseudo-Gibbs effect to a certain extent, and there are some drawbacks, which need to be further developed and improved.

In order to make up for the lack of analysis of the overall structure and the complexity of the operation in the traditional BM3D algorithm, this paper firstly establishes a wave-domain harmonic filter diffusion model to improve the BM3D denoising algorithm, and extracts the block matching pre-estimation through wavelet decomposition. The high-frequency part of the image is filtered. In order to avoid edge blurring, the Laplacian Gaussian algorithm is used to construct a new operator and bring into the diffusion model. Finally, the wavelet coefficients are reconstructed to obtain the final denoised image. Due to the wavelet method of non-geometric transformation The anisotropic elements at the edge line position are limited when extracting transform coefficients. The multiscale geometric analysis method using shearlet transform can improve the edge protection ability. A block matching denoising based on non-subsampling shearlet (NSST) is proposed. Model. In Section II, the paper proposes a new model 1, and proposes an improved model 2 for the shortcomings of the model 1 in Section III, and proves the superiority of the two new models through experimental renderings and experimental data. Finally, concluding observations are made in Section IV.

2 Block Matching Based Gaussian Harmonic Filtering

At present, many improved BM3D can effectively denoise, but the defects that lead to blurred edge details need to be improved. In order to make up for the lack of analysis of the overall structure and the complexity of the current image denoising algorithm, this section establishes a harmonic filtering diffusion model to improve the BM3D image denoising algorithm. The algorithm first combines similar two-dimensional image blocks into 3D arrays by using the traditional Euclidean distance method, and then converts the filtered 3D arrays into predictor data. Secondly, wavelet decomposition transform is used to extract the high frequency part of the predictor image and filter it. In order to avoid edge blurring, Laplace-Gaussian algorithm is used to construct a new operator into the diffusion model. Finally, wavelet reconstruction is performed to obtain the final approximation of the original image.

2.1 Theoretical Implementation of the Algorithm

(1) Preliminary denoising

The reference image block of $x, y \in R$ is defined as $x, y \in R$, where $B_{x,y}$ is a matching block positioned in the noisy image $I_{0(x,y)}$. An image with a similar block is searched from another region similar to the region of the center pixel point of the current reference block by using the Euclidean distance measurement criterion, as shown in Eq. (1):

$$d\left(B_{x_R,y_R}, B_{x,y}\right) = N_1^{-2} \left\| \gamma(\Gamma_{2D}\left(B_{x_R,y_R}\right) - \gamma(\Gamma_{2D}\left(B_{x,y}\right)) \right\|_2^2 . \quad (1)$$

Where B_{x_R,y_R}, $B_{x,y}$ are image blocks of size $N_1 \times N_1$. Parameter Γ_{2D}, representing a two-dimensional linear transform performed by DCT, that is, the original subimage $N \times N$ is replaced by subimage $2N \times 2N$ with sym-

metric pixels. In addition, the transform coefficient will only have the cosine term of the real number, thus avoiding the Gibbs phenomenon. γ is a threshold operator defined as follows:

$$\gamma\left(\lambda,\lambda_{thr}\right)=\begin{cases}\lambda & \left|\lambda\right|>\lambda_{thr}\\ 0 & \left|\lambda\right|\le\lambda_{thr}\end{cases}, \tag{2}$$

Where τ_{match} is the maximum distance for searching similar blocks of an image block, and the result obtained by block matching using Eq. (1) is defined as follows:

$$S_{x_R,y_R}=\left\{x,y\in R\middle|d(B_{x_R,y_R},B_{x,y})<\tau_{match}\right\}. \tag{3}$$

The similar blocks in set S_{x_R,y_R} are combined and stacked into a $N_1\times N_1\times S_{x_R,y_R}$ 3D array, and then a normalized 3D linear transform is performed, followed by a 3D inverse transform to obtain a preliminary approximation of the matched blocks:

$$\hat{I}_{S_{xR,yR}}=\Gamma_{3D}^{-1}\left(\gamma\left(\Gamma_{3D}\left(I_{0S_{xR,yR}}\right)\right)\right), \tag{4}$$

Processing results $\hat{I}_{S_{xR,yR}}$ in Eq. (4) are stacked as $\hat{I}_{\mathrm{x,y}}^{x_R,y_R}$, where x,y is the position of the estimated block, and x_R,y_R represents the position of a similar block. The weighted average of pixel points of all the image blocks are calculated to avoid overlapping of the estimates [19], thereby obtaining a preliminary approximation of the original image:

$$\hat{I}_{basic}=\frac{\sum_{x,y\ R}\sum_{xm,ym\ S_{xR,yR}}\omega_{xR,yR}\hat{I}_{xm,ym}^{x_R,y_R}}{\sum_{x,y\ R}\sum_{xm,ym\ S_{xR,yR}}\omega_{xR,yR}\psi_{xm,ym}}, \tag{5}$$

Where $\hat{I}_{basic}$ is the processed image, $\psi_{xm,ym}$ is the feature function positioned at block (xm,ym), and ω_{x_R,y_R} represents the weight assigned by the group estimate; it is defined as

$$\omega_{x_R,y_R}=\begin{cases}\sigma^{-2}N_{x_R,y_R}^{-1} & N_{x_R,y_R}\ge 1\\ 1 & N_{x_R,y_R}<1\end{cases}, \tag{6}$$

Where N_{x_R,y_R} represents the number of nonzero coefficients after normalization and linear transform of a 3D array, as defined in Eq. (3).

(2) Final denoising

Because the noise and edge details of the image mainly exist in the high-frequency region of the image, the result obtained by Eq. (5) is decomposed using the Mallat algorithm to extract the high-frequency part of the detailed information (horizontal direction h, vertical direction v, and diagonal direction d) in the predictor image, and the high-frequency coefficients are processed through diffusion filtering. The diffusion function proposed by Perona and Malik [1] has the ability of edge sharpening and forward diffusion as well as backward diffusion; thus, it can be used as a diffusion model to remove noise. The specific PM models are as follows:

$$\begin{cases}\dfrac{\partial I}{\partial t}=div\{c\left[W\times\left(\left|\nabla\hat{I}_{basic}\right|\right)\right]\nabla\hat{I}_{basic}\}\\ \hat{I}_{final}\left(x,y,0\right)=I_{basic}\end{cases}, \tag{7}$$

Where $\hat{I}_{basic}$ is the preliminary estimated BM3D image, W represents the wavelet transform decomposition of the image, and $c(g)$ represents a decreasing function related to gradient information. This function is used to control the diffusion degree of each position in the diffused image and is consistent with the definition of the PM model, i.e., $c(x) = \exp(-\left(\frac{x}{k}\right)^2)$, where k is a threshold coefficient. Edge blurring occurs during wave domain transform, and the edge corners are easily smoothened. The second derivative of the Laplace operator is very sensitive to noise, and its zero-crossing property is used to locate the image in edge detection. The Laplace operator can be derived as follows: a new filter can be constructed by combining Laplace–Gaussian stress distribution balance with gradient operator and can be expressed as:

$$\nabla \hat{I}_{basic} + \nabla^2 I_{basic} = \sqrt{I_x^2 + I_y^2} + \frac{\partial^2 I}{\partial x^2} + \frac{\partial^2 I}{\partial y^2} \quad . \tag{8}$$

By substituting Eq. (8) into Eq. (7), a new diffusion model is established:

$$\begin{cases} \dfrac{\partial I}{\partial t} = c(\cdot)\, div\{c\left[W\left(\left|\nabla \hat{I}_{basic} + \nabla^2 I_{basic}\right|\right)\right]\nabla I_{basic}\} \\ \hat{I}_{final}(x, y, 0) = I_{basic} \end{cases} , \tag{9}$$

Where $\mathrm{c}(\bullet) = \mathrm{c}\left(\left|G_\sigma * \nabla \hat{I}_{basic}\right|\right)$ is used to enhance the edge of the image and control the diffusion velocity. G_σ is Gaussian kernel function and is defined as

$$G_\sigma = \frac{1}{\sqrt{2\pi\sigma}} e^{-\frac{\left(x^2+y^2\right)}{4\sigma}} \quad . \tag{10}$$

To solve Eq. (9), a numerical discretization scheme can be used to simplify the implementation of the algorithm, and the grid coordinates are defined as $Net = (il, jl, \Delta t)$, where l is the grid length and Δt is the time-step size. Therefore,

$$\begin{cases} I_{i,j}^n = I \cdot Net \\ a_{i,j}^n = \mathrm{c}\left(\left|G_\sigma * \nabla \hat{I}_{basic}\right|\right) \cdot Net \\ b_{i,j}^n = c\left[W \times \left(\left|\nabla \hat{I}_{basic} + \nabla^2 I_{basic}\right|\right)\right] \cdot Net \end{cases} . \tag{11}$$

Definition of $I_{basic}^{\sim} = \left[W\left(\left|\nabla \hat{I}_{basic} + \nabla^2 I_{basic}\right|\right)\right]$:

$$\begin{aligned} & div\left[c\left(I_{basic}^{\sim}\right)\nabla \hat{I}_{basic}\right] \\ & = \frac{\partial}{\partial x}\left[c\left(I_{basic}^{\sim}\right)\frac{\partial I}{\partial x}\right] + \frac{\partial}{\partial y}\left[c\left(I_{basic}^{\sim}\right)\frac{\partial I}{\partial y}\right] \\ & = \frac{\partial}{\partial x}\left(c\left(I_{basic}^{\sim}\right)\right)\frac{\partial I}{\partial x} + c\left(I_{basic}^{\sim}\right)\frac{\partial^2 I}{\partial x^2} + \frac{\partial}{\partial y}\left(c\left(I_{basic}^{\sim}\right)\right)\frac{\partial I}{\partial y} + c\left(I_{basic}^{\sim}\right)\frac{\partial^2 I}{\partial y^2} \end{aligned} \quad . \tag{12}$$

Thus, the discrete expression of $\frac{\partial I}{\partial x}$ is $\frac{I_{i+1,j}-I_{i-1,j}}{2l}$; the discrete expression of $\frac{\partial^2 I}{\partial x^2}$ is $\frac{I_{i+1,j}-2I_{i,j}+I_{i-1,j}}{l^2}$; the first term of Eq. (12), $\frac{\partial}{\partial x}\left[c\left(I_{basic}^{\sim}\right)\frac{\partial I}{\partial x}\right]$ is obtained as Eq. (13); and the discrete expression of $\frac{\partial}{\partial y}\left[c\left(I_{basic}^{\sim}\right)\frac{\partial I}{\partial y}\right]$ obtained by the same method is expressed as Eq. (14). By substituting the discrete expressions in Eqs. (13) and (14) into the diffusion equation, Eq. (9), the implicit difference scheme is obtained as Eq. (15):

$$\frac{1}{2l^2}\begin{bmatrix}\left(b_{i-1,j}^n+b_{i,j}^n\right)I_{i-1,j}^{n+1}\\-\left(2b_{i,j}^n+b_{i-1,j}^n+b_{i+1,j}^n\right)I_{i+1,j}^{n+1}\\+\left(b_{i,j}^n+b_{i+1,j}^n\right)I_{i+1,j}^{n+1}\end{bmatrix}, \tag{13}$$

$$\frac{1}{2l^2}\begin{bmatrix}\left(b_{i,j-1}^n+b_{i,j}^n\right)I_{i,j-1}^{n+1}\\-\left(2b_{i,j}^n+b_{i,j-1}^n+b_{i,j+1}^n\right)I_{i,j+1}^{n+1}\\+\left(b_{i,j}^n+b_{i,j+1}^n\right)I_{i,j+1}^{n+1}\end{bmatrix}, \tag{14}$$

$$\frac{I_{i,j}^{n+1}-I_{i,j}^n}{\Delta t}=\frac{1}{2l^2}a_{i,j}^n\begin{bmatrix}\left(b_{i-1,j}^n+b_{i,j}^n\right)I_{i-1,j}^{n+1}+\left(b_{i,j-1}^n+b_{i,j}^n\right)I_{i,j-1}^{n+1}\\+\left(b_{i,j}^n+b_{i+1,j}^n\right)I_{i+1,j}^{n+1}+\left(b_{i,j}^n+b_{i,j+1}^n\right)I_{i,j+1}^{n+1}\\+\left(4b_{i,j}^n+b_{i-1,j}^n+b_{i,j-1}^n+b_{i+1,j}^n+b_{i,j+1}^n\right)I_{i,j}^{n+1}\end{bmatrix}. \tag{15}$$

By defining $\mathbf{M}_l(I^n)=[a_{ij}(I^n)]$, Eq. (16) can be written in matrix form and further simplified to

$$\frac{I^{n+1}-I^n}{\Delta t}=\mathbf{M}_l(I^n)I^{n+1}\ . \tag{16}$$

The evolutionary equation is

$$I^{n+1}=\left(1-\Delta t\mathbf{M}_l(I^n)\right)^{-1}I^n\ . \tag{17}$$

(3) Specific steps of the algorithm are as follows:

Step 1: Parameter initialization. The noisy image is divided into image blocks of $N_1\times N_1$ different sizes, and similar blocks of the reference blocks are found and collected as set S_{x_R,y_R}, according to the conventional Euclidean distance criterion.

Step 2: Normalize the stacked 3D array through linear transform filtering on set S_{x_R,y_R}, and obtain matched block estimation $\hat{I}_{S_{x_R,y_R}}$ through inverse transform.

Step 3: Obtain preliminary estimate $\hat{I}_{basic}$ of the original image according to the weighted average of $\hat{I}_{S_{x_R,y_R}}$.

Step 4: Use wavelet decomposition to extract the high-frequency components of $\hat{I}_{basic}$ obtained in Step 3, and use the diffusion model of Eq. (9) to denoise the image.

Step 5: Reconstruct the high- and low-frequency coefficients processed in Step 4 to obtain the final approximation, $\hat{I}_{final}$, of the original image.

2.2 Model Verification and Analysis

To verify the noise removal effect of new model 1 proposed in this section, add Gaussian noise of intensity 20 to the original image, MATLAB simulation software was used to conduct Gaussian noise removal analysis to verify the feasibility of this algorithm. The filter model was used to set the time step, $\Delta t = 0.2$, and iteration times, $n = 7$. In wavelet threshold denoising, natural images, Lena, Barbara, Dxy and Tsg (pixel size of 512 × 512) were denoised with the same parameters. WHT, PM, NLM, BM3D, and the new algorithm were used to smoothen the denoising. The denoising effect graphs are shown in Fig. 1, Fig. 3, Fig. 5, and Fig. 7. The effectiveness of the algorithm was compared and evaluated through subjective visibility observations, peak signal-to-noise ratio (PSNR), and objective indicators of structural similarity (SSIM) (Table 1). To accurately display the edge information before and after filtering, a Canny operator was used to detect the edge of the denoising effect image of each algorithm, and the results are shown in Fig. 2, Fig. 4, Fig. 6, and Fig. 8.

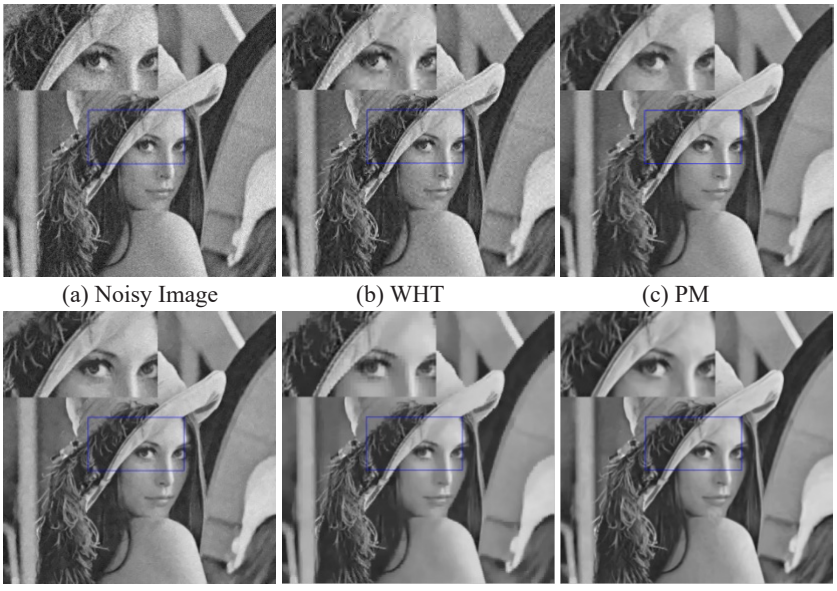

(a) Noisy Image (b) WHT (c) PM

(d) NLM (e) BM3D (f) New Method 1

Fig. 1. Filter denoising effect diagram for different methods (Lena)

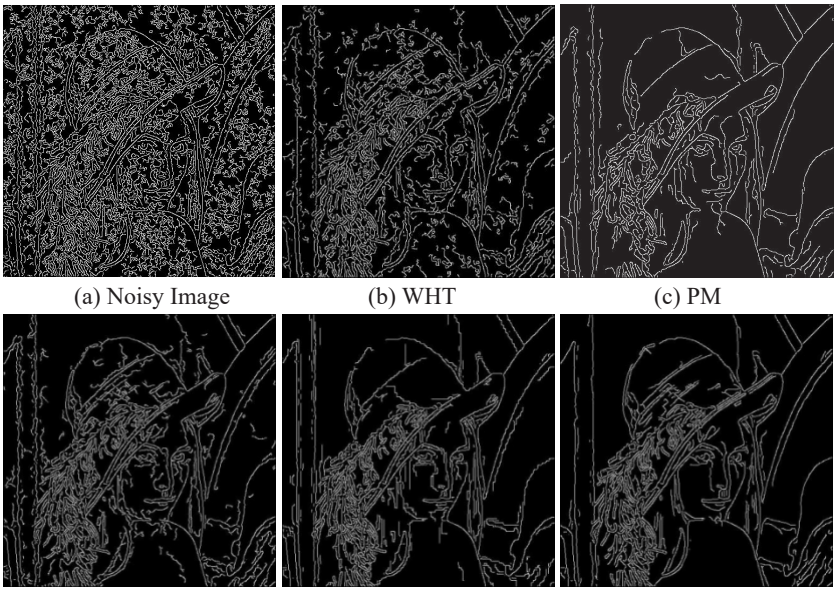

(a) Noisy Image (b) WHT (c) PM

(d) NLM (e) BM3D (f) New Method 1

Fig. 2. Smooth edge extraction diagram for different denoising models (Lena)

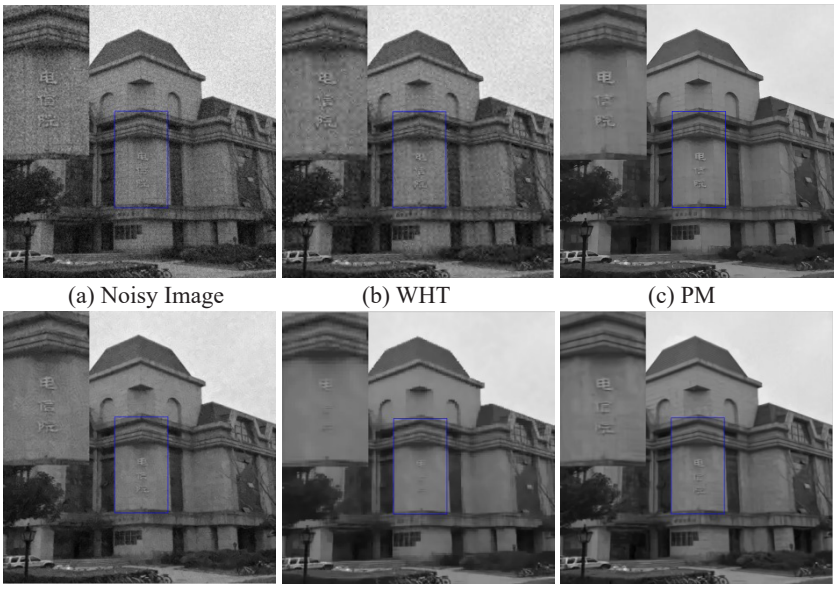

(a) Noisy Image (b) WHT (c) PM

(d) NLM (e) BM3D (f) New Method 1

Fig. 3. Filter denoising effect diagram for different methods (Dxy)

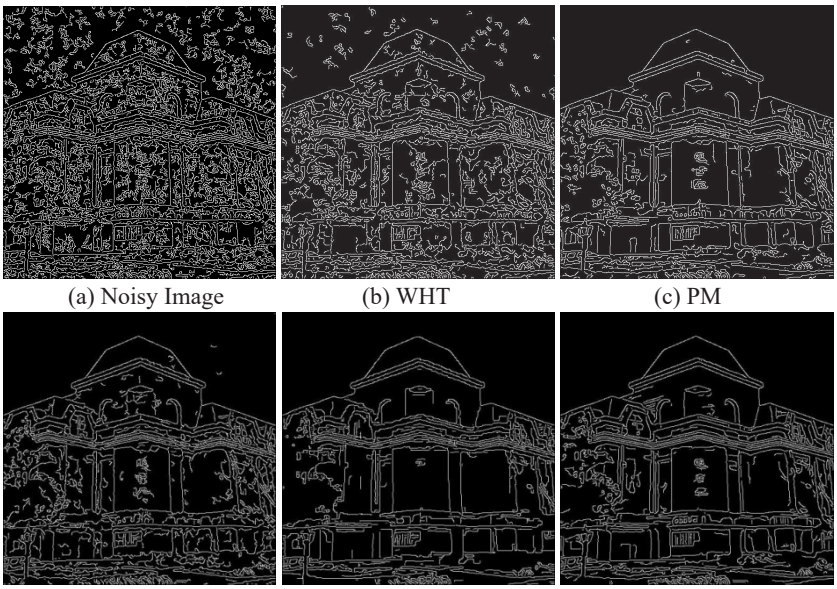

(a) Noisy Image (b) WHT (c) PM

(d) NLM (e) BM3D (f) New Method 1

Fig. 4. Smooth edge extraction diagram for different denoising models (Dxy)

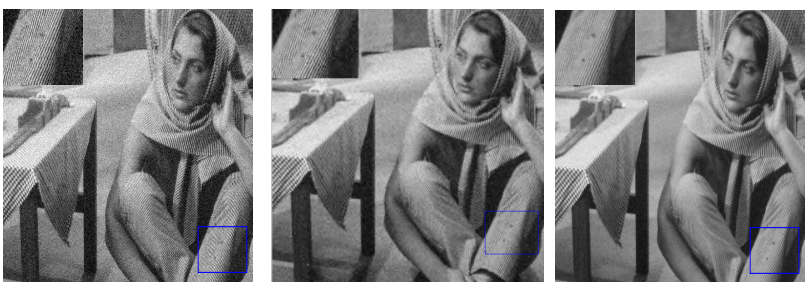

(a) Noisy Image (b) WHT (c) PM

(d) NLM (e) BM3D (f) New Method 1

Fig. 5. Filter denoising effect diagram for different methods (Barbara)

(a) Noisy Image (b) WHT (c) PM

(d) NLM (e) BM3D (f) New Method 1

Fig. 6. Smooth edge extraction diagram for different denoising models (Barbara)

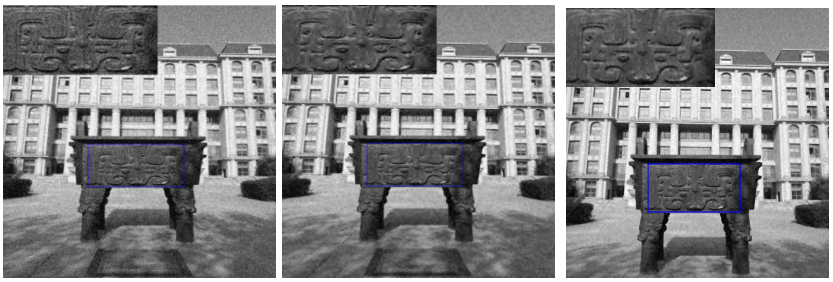

(a) Noisy Image (b) WHT (c) PM

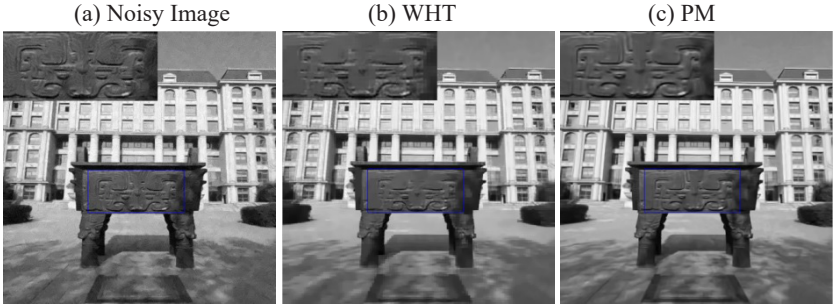

(d) NLM (e) BM3D (f) New Method 1

Fig. 7. Filter denoising effect diagram for different methods (Tsg)

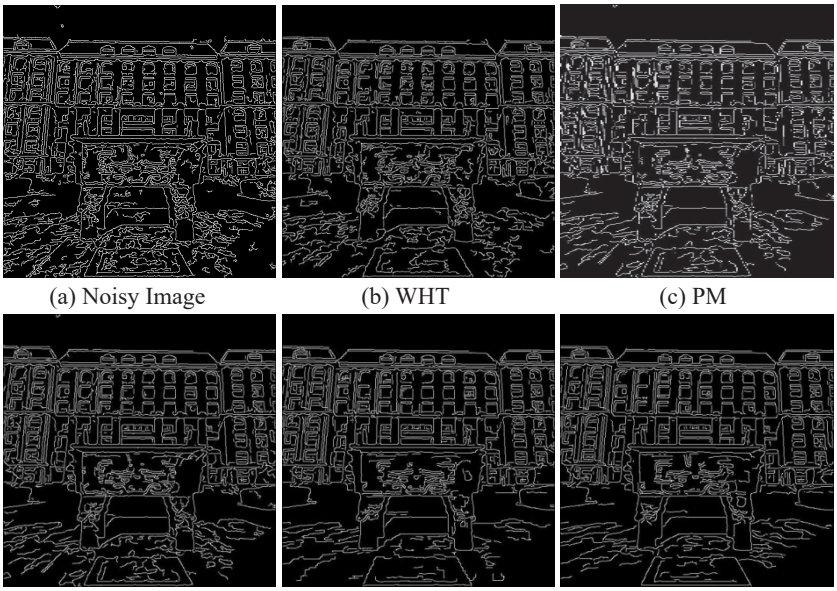

(a) Noisy Image (b) WHT (c) PM

(d) NLM (e) BM3D (f) New Method 1

Fig. 8. Smooth edge extraction diagram of different denoising models (Tsg)

The denoising effect diagram and local method diagram of the natural image Lena, Dxy, Barbara, Tsg are shown in Fig. 1 to Fig. 8. Fig. 1(b), Fig. 3(b), Fig. 5(b), and Fig. 7(b) show that visibility of the WHT method, it can be found that the smoothing effect of the WHT method is relatively poor from the visual effect, because this method will remove the wavelet coefficients in the high-frequency subband as noise coefficients during denoising, thereby losing texture information. Fig. 1(c), Fig. 3(c), Fig. 5(c), and Fig. 7(c) show that the gradient value of the PM model is extremely susceptible to the influence of noise points, and it is easy to produce a staircase effect. Fig. 1(d), Fig. 1(e), Fig. 3(d), Fig. 3(e), Fig. 5(d), Fig. 5(e), and Fig. 7(d), Fig. 7(e) show that that visibility of the BM3D method is more improved than that of the NLM filtering method. This is demonstrated from the edge-filtering detection images, shown in Fig. 2(e), Fig. 4(e), Fig. 6(e), and Fig. 8(e). However, Fig. 3(e) shows that the BM3D method does not accurately represent complex images, and when the noise variance is large, many "mosaics" phenomena are prone to occur, leading to blurring of important details and lack of the grasping of the overall structure. Therefore, the source information is lost in the edge detection result diagram in Fig. 6(e). Fig. 3(f) shows that the new method can improve the effect of the denoising effect of the Dxy image, and it can effectively recover the information of the wall surface texture, that is, the word "Telecommunication House," and the surrounding wall surface texture information.

The Barbara image of Fig. 5(f) shows the stripe information of the trouser foot and tablecloth, and the Tsg image of Fig. 7(f) shows the texture pattern on the tripod. Compared with the previous algorithm, the texture information is well preserved and slight residual noise is obtained; this was proved by the results of the Canny edge detection image shown in Fig. 8(f). In addition, the evaluation index in Table 1 is consistent with the visibility effect of the filtering result.

Table 1. Comparison of PSNR and SSIM for different images using different denoising models

		Noisy image	WHT	PM	NLM	BM3D	New
Lena	PSNR	22.0442	25.2876	27.8168	28.2839	29.9878	33.0076
	SSIM	0.3421	0.5840	0.6310	0.6566	0.8213	0.9887
Dxy	PSNR	22.3339	25.0643	27.6380	28.2220	29.6441	32.4449
	SSIM	0.4114	0.5799	0.6086	0.6577	0.8071	0.9992
Barbara	PSNR	22.0442	23.9802	25.2078	27.4264	28.7015	31.7782
	SSIM	0.3421	0.6072	0.7082	0.7238	0.8376	0.9899
Tsg	PSNR	23.3026	24.0988	25.6755	27.2801	28.5177	30.9052
	SSIM	0.3714	0.6022	0.6985	0.7189	0.8381	0.9904

The comparison of the evaluation indexes in Table 1 shows that the new method is not higher than the PSNR and SSIM of the previous methods; however, the improved algorithm is superior to the previous methods only from the perspective of visibility.

3 Block Matching Denoising of Non-Subsample Shearlet Transform

Because the wavelet method of a nongeometric transform relies on isotropic elements at all scales when extracting transform coefficients and has a limitation for anisotropic elements at edge lines, the Gibbs effect is easily produced. In order to improve the preservation of edge detail information by wavelet transform algorithm. This section fully studies the theoretical knowledge of Shearlet, NSST and BM3D. The performance of image denoising depends largely on the ability of sparse representation of images. In Reference [17], a Shearlet geometric transform for constructing sparse representation of multidimensional functions using a frame of an affine system with synthetic expansion is proposed. In Reference [20], He. et al proposes a new method for denoising using deep neural network NSST-UNET to improved BM3D, adopt NSST coding layer and skip connection design based on multi-scale convolution module to identify edges and smooth regions of noisy images, and then use improved BM3D to complete denoising in two steps.

Theoretically, the multiscale geometric analysis method of Shearlet transform has an optimal sparse representation of the image. The digital implementation of the transform is simple, effectively captures multiscale and multidirectional information, and has good directional sensitivity and edge-holding ability. Therefore, a block-matching denoising model based on non-subsample Shearlet transform (NSST) is proposed in this section. The new model first predicts the scaling threshold according to the statistical properties of the histogram, performs hard threshold filtering on high frequency subbands, and performs block-matched 3D filtering on the decomposed low frequency subband coefficients. All processed subband coefficients are inverse transformed and reconstructed to get denoised image. New model can effectively remove image noise while retaining edge details and other information.

3.1 Shearlet Transform and Its Multiscale Geometric Analysis

According to the Shearlet theoretical analysis, the Shearlet transform into the frequency domain is tightly supported and has good localization characteristics. The calculation steps of the discrete shear wave transform can generally be divided into two processes: multi-scale decomposition and direction localization. The Laplacian pyramid algorithm calculates the resolution in the discrete domain, completes multi-scale decomposition, and decomposes K high-frequency images and one low-frequency image through K-level downsampling, which can realize multi-scale analysis; in addition, it is necessary to construct scale and the window function of the direction change to realize the localization of the direction to obtain the high frequency components in each direction. However, since the shearlet transform adopts the down-sampling operation, it is easy to produce phase distortion due to the lack of translation invariance when the coefficients are reconstructed. Pseudo-Gibbs phenomenon caused by recovering the edges of the image. That is, in the process of direction localization, the Cartesian coordinate system is used to replace the pseudo-polarization network system, the Fourier transform is calculated by the pseudo-polar coordinate system and the band-pass filtering is performed, and then the two-dimensional inverse Fourier transform method is used, and finally the shear wave transform coefficients in all directions are obtained. Fig. 9 shows a schematic diagram of multi-directional decomposition of NSST, in which $C_k^d(x,y)$ represents the set of shear wave high-frequency subband coefficients of the two-dimensional image (x,y), and $C_k^a(x,y)$ represents the set of separated low-frequency sub-band coefficients.

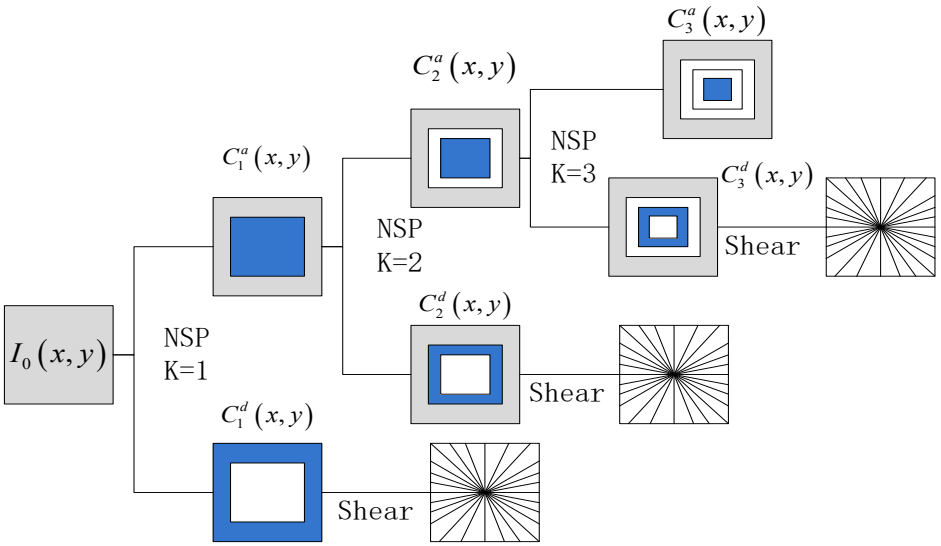

Fig. 9. NSST multidirectional explosion schematics

3.2 Selection of New Method Threshold

In this section, the NSST method is introduced to generate a large number of Shearlet coefficients in the process of decomposing noisy images; thus, it is necessary to separate the noise in sub-bands from the original signal. If the threshold value of coefficient processing is too large, the edge structure will be lost; however, if the value is too low, the noise will remain; thus, it is important to select an appropriate threshold value. Because Donoho's shrinkage threshold equation is $T=\sigma\sqrt{2\ln N}$, the conventional wavelet threshold denoising method achieves good results in the asymptotic sense. With the development of the later theory, many scholars have proposed many improved methods based on Donoho threshold according to the hypothesis of model distribution. Moreover, the inadequacy of data and correlation aggravates the uncertainties in the process of noise reduction as an inverse problem. Therefore, the key to successful noise reduction lies in understanding the prior information of the signal and the mechanism and characteristics of noise [21]. Chang [22] assumed that the wavelet coefficients obey the generalized Gaussian distribution, and defined the shrinkage threshold as $T=\sigma^2/\sigma$, which is called the Bayesian threshold. Under the assumption that the wavelet coefficients obey Laplace distribution, Moulin [23] proposed a Mapshrink threshold based on the Laplace distribution λ. In addition, the GCV threshold criterion [24], as shown in Eq. 18, is increasingly becoming popular among scholars. This method does not need to estimate the noise variance and can be used directly:

$$T_{GCV}=\min\left|\frac{1}{N}\sum\frac{(w-\hat{w})^2}{(N_0/N)^2}\right|, \tag{18}$$

Where N is the number of coefficients after wavelet transform, N_0 is the number of coefficients representing the signal being set to zero, w and $\hat{w}$ represent the coefficient containing noise and the coefficients after threshold shrinkage processing are represented. Vidakovic et al. processed the wavelet coefficients with hard thresholds combined with the different characteristics of the "main signal" coefficients and "main noise" coefficients in the cross-scale distribution based on Bayes framework. In image processing, the choice of threshold value still needs to depend on the specific situation. Generally, the denoising should be limited according to the known characteristics of the signal to avoid the occurrence of pathological problems. Therefore, we define $C_k^d(x,y)$ as the set of high-frequency sub-band coefficients of the shear wave as a two-dimensional image (x,y); $C_k^a(x,y)$ represents the set of separated low-frequency sub-band coefficients. According to the hard threshold function,

$$\hat{C}_k^d(x,y)=\begin{cases}C_k^d(x,y) & C_k^d(x,y)\geq T\\ 0 & C_k^d(x,y)<T\end{cases}, \tag{19}$$

Where $\hat{C}_k^d(x,y)$ represents the coefficients of the shear wave sub-bands after the conversion processing are represented and T represents the histogram threshold value. The statistical characteristics of the image can be accurately reflected by histogram, that is, the intensity distribution of the gray value in the image pixels can be represented by the intensity distribution. This method has the invariance of translation, scaling, rotation, etc., and the computational cost is small. Here, the initial threshold T_0 is used to divide the coefficient range into equal-sized intervals B_1 B_2 B_3 to construct histograms, and to calculate the mean values, i.e., $Mean_1, Mean_2, Mean_3$, of the number of points in each type of dataset. Threshold T is defined as

$$T=1/3\left(Mean_1+Mean_2+Mean_3\right), T<T_0\ . \tag{20}$$

3.3 Concrete Step of Algorithm

Based on the above-mentioned theoretical analysis, the experimental steps for this section of the model can be obtained, and the implementation block diagram is shown in Fig. 10.

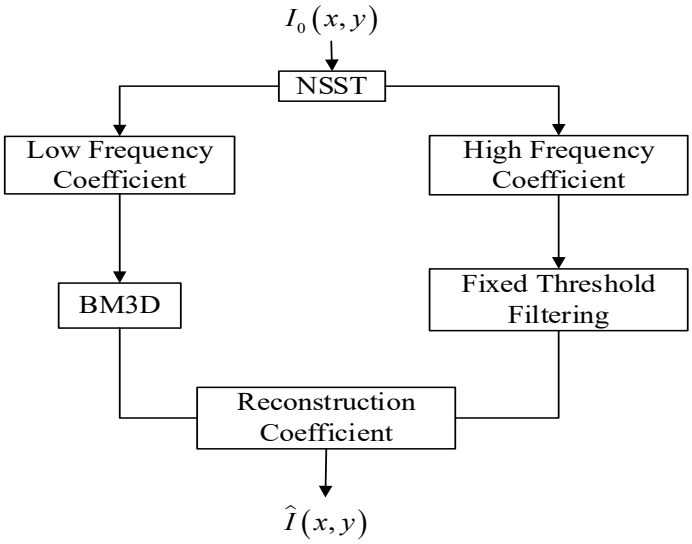

Fig. 10. Algorithm framework for the new model

Step 1: Three-layer NSST transform is performed on the image containing noise, namely, ST coefficients in each scale direction are obtained;

Step 2: Block-matched 3D filtering is performed on the decomposed low-frequency sub-band coefficients to obtain the processed coefficients, $C_k^a(x\ y)$;

Step 3: Performing hard threshold filtering on the high frequency sub-band according to histogram estimation to obtain the processed coefficients, $C_k^d(x,y)$;

Step 4: Finally, the ST coefficients processed in Step 3 and Step 4 are inversely transformed to obtain the de-noised image.

3.4 Model Verification and Analysis

To verify the denoising effect of new model 2 based on shear wave transform, the MATLAB simulation software and ShearLab toolkit are used to verify the feasibility of the new algorithm, The comparison algorithms include

BM3D, shearlet, hard threshold NSST method (NSST-hard) and the new algorithm in this chapter. The denoising experiments of Lena, Dxy, Barbara, and Tsg (pixel sizes are 512 × 512) are conducted with the same parameters. The denoising effect diagram is shown in Fig. 11 to Fig. 18. We performed a subjective visibility comparison with the denoising effect diagram in Fig. 19 according to shear wave denoising. Objectivity indexes, such as PSNR and structural similarity (SSIM) after denoising in different variance, were used to evaluate the effectiveness of the algorithm, as shown in Table 2. The comparison of Fig. 13, Fig. 15 and Fig. 17 shows that the new algorithm in this section significantly improves many artifacts and visibility in shear wave denoising. The texture of the ground and stone column in Fig. 13(a) Lena show that the details of the image is well preserved. In addition, the tablecloths and trouser legs of Barbara in Fig. 13(c) show that the Gibbs phenomenon affects visibility during reconstruction. Observing Fig. 15 and Fig. 16, some texture details are lost after NSST-hard denoising, and some directional textures on the hat in the Lena image and some direction textures on the pants in the Barbara image are lost. The window edges and shadows in the Tsg image of Fig. 17(d) are not affected; however, some blurring still exists in the distant steps, which should be further improved. Overall, the new algorithm retains the edge detail information relatively well while effectively denoising. To better display the filtered edge information, the Canny operator was used to detect the edge of the denoising image of each algorithm, and the results are shown in Fig. 12, Fig. 14 , Fig. 16 and Fig. 18. The noise filtering are relatively clean, and the edge texture structure have a certain degree of protection. The denoising performance and texture feature protection of this difficult point was broken through.

(a) Lena (b) Dxy (c) Barbara (d) Tsg

Fig. 11. Effect diagram of different images denoised by BM3D

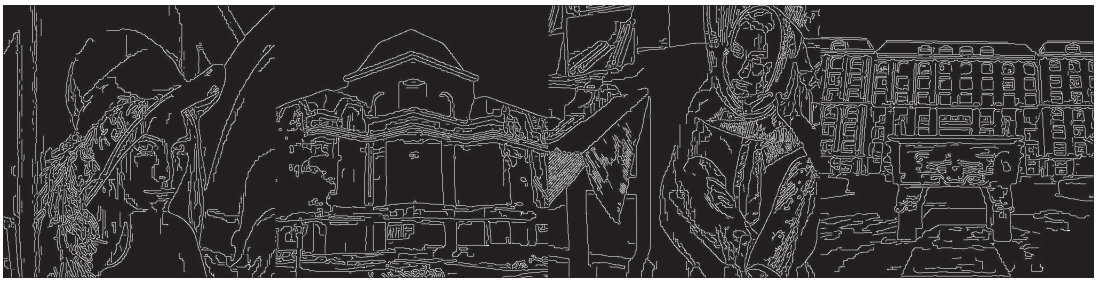

(a) Lena (b) Dxy (c) Barbara (d) Tsg

Fig. 12. Edge detection diagram of different images denoised by BM3D

(a) Lena (b) Dxy (c) Barbara (d) Tsg

Fig. 13. Effect diagram of different images denoised by Shearlet

(a) Lena (b) Dxy (c) Barbara (d) Tsg

Fig. 14. Edge detection diagram of different images denoised by Shearlet

(a) Lena (b) Dxy (c) Barbara (d) Tsg

Fig. 15. Effect diagram of different images denoised by NSST-hard

(a) Lena (b) Dxy (c) Barbara (d) Tsg

Fig. 16. Edge detection diagram of different images denoised by NSST-hard

(a) Lena (b) Dxy (c) Barbara (d) Tsg

Fig. 17. Effect diagram of different images denoised by the new algorithm 2 in this section

(a) Lena (b) Dxy (c) Barbara (d) Tsg

Fig. 18. Edge detection diagrams of different images denoised by new algorithm 2 in this section

The comparison of the evaluation indexes in Table 2 shows that the improved algorithm is not much higher than the PSNR of the shear wave transform method; however, the new method is superior to the shear wave transform method only from the perspective of visibility. The complexity of the algorithm should be further optimized. Fig. 19 is a simulation diagram showing the PSNR of the experimental image processed by the new algorithm in this section and the PSNR of the noisy image.

Table 2. Comparison of objectivity of denoising methods under different variances

Method	σ		Lena	Dxy	Barbara	Tsg
BM3D	10	PSNR	33.7390	32.9046	31.6980	31.9012
		SSIM	0.8979	0.9074	0.8562	0.8599
	20	PSNR	29.9878	29.6441	28.7015	28.5177
		SSIM	0.8213	0.8071	0.8376	0.8381
	30	PSNR	28.0378	27.2511	26.0317	25.7390
		SSIM	0.6993	0.6799	0.6298	0.6421
	40	PSNR	25.0024	25.3094	24.2015	23.9076
		SSIM	0.5997	0.6010	0.5783	0.5590
Shearlet	10	PSNR	35.0076	34.7524	33.7449	33.4231
		SSIM	0.9024	0.8905	0.9125	0.9172
	20	PSNR	31.8955	31.1490	30.0313	29.5293
		SSIM	0.8122	0.7481	0.8558	0.8540
	30	PSNR	30.0041	29.1557	27.7397	27.2708
		SSIM	0.7113	0.6661	0.7705	0.7451
	40	PSNR	27.0324	27.2104	26.1319	25.2825
		SSIM	0.6257	0.6149	0.7012	0.6816
NSST-hard	10	PSNR	35.0133	34.8085	33.6997	33.5078
		SSIM	0.9101	0.9001	0.9134	0.9176
	20	PSNR	31.9377	31.2842	30.0197	29.7960
		SSIM	0.8359	0.8023	0.8213	0.8601
	30	PSNR	30.0097	29.1922	27.8023	27.3975
		SSIM	0.7220	0.6676	0.7735	0.7590
	40	PSNR	27.0976	27.2198	26.2370	25.2980
		SSIM	0.6985	0.6571	0.7124	0.7038
New Method 2	10	PSNR	35.0098	34.9554	33.6561	33.9531
		SSIM	0.9016	0.8903	0.9160	0.9258
	20	PSNR	33.0783	32.7965	31.1167	30.7842
		SSIM	0.8499	0.8316	0.8566	0.8562
	30	PSNR	30.1341	29.2282	28.0874	27.6865
		SSIM	0.8001	0.7826	0.7925	0.7894
	40	PSNR	27.2652	27.2483	26.6362	25.3351
		SSIM	0.7874	0.7459	0.7371	0.7451

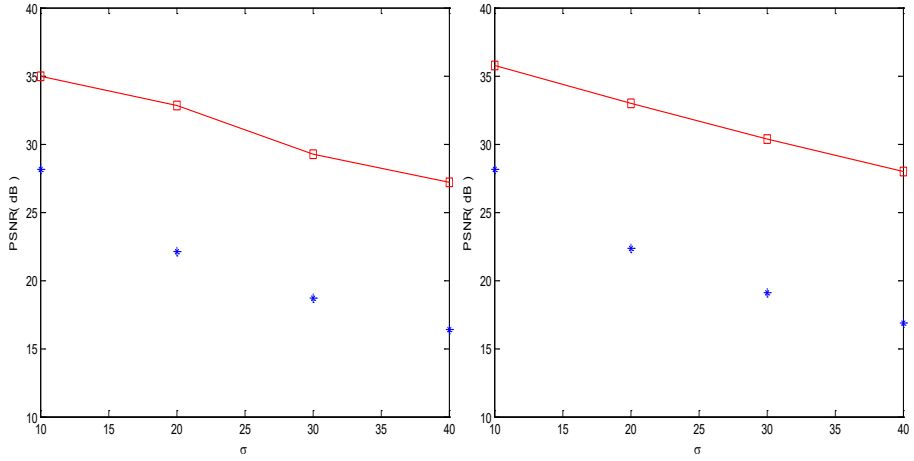

(a) Lena (b) Dxy

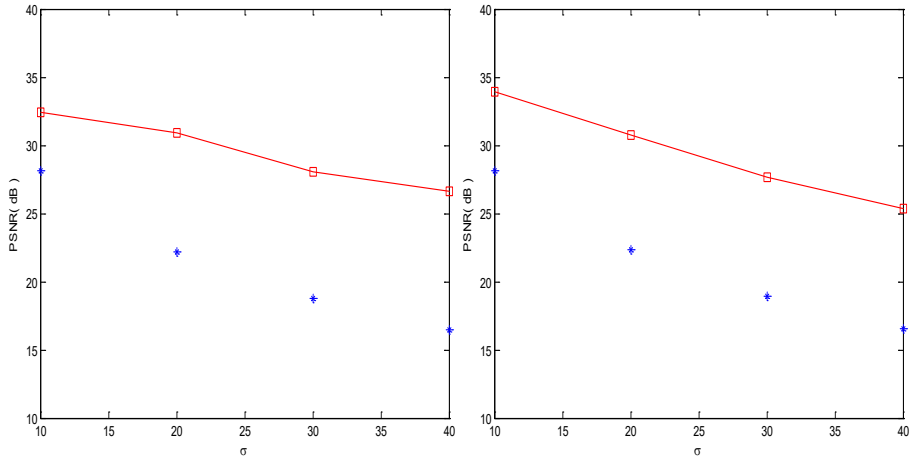

(c) Barbara (d) Tsg

Fig. 19. PSNR simulation comparison diagram after noise removal for new algorithm 2

4 Conclusion

Based on the theoretical analysis of transform domain and block matching denoising methods, a diffusion model based on harmonic filtering in the wave domain was proposed to improve the BM3D technique. The algorithm extracts a high-frequency part of the predictor image through wavelet decomposition and filtering. Considering the possibility of edge blurring, the Laplace-Gaussian algorithm was used to construct the diffusion model. Subsequently, wavelet reconstruction was performed to obtain the final approximation of the original image. To better display the edge information before and after filtering, a Canny operator was used to verify and compare the edge display effect of each algorithm. Because the wavelet method of non geometric transform relies on isotropic elements appearing in all scales when extracting transform coefficients, it has limitations for anisotropic elements at the edge line position, which is easy to produce Gibbs effect. Therefore, a block matching denoising model based on NSST was proposed by the theoretical analysis of shear waves. The coefficients of each scale direction were obtained using a three-layer NSST transform, by block matching 3D filtering of the decomposed low-frequency sub-band coefficients. And the coefficients were obtained through hard threshold filtering of the high-frequency sub-band according to histogram estimation, and finally the denoised image was obtained through an inverse transform. The PSNR of the new model has been significantly improved, which can not only effectively remove the noise in the image, but also retain the details such as edge texture, which is conducive to the acquisition of image feature information. However, some simple and effective transformation methods need to be optimized and improved, and the selection of the best threshold should also be further developed and improved.

5 Acknowledgement

This work was supported by the National Natural Science Foundation of China (11202106, 61302188). This work was supported by the Research and Application Center of Intellisense Technology of IOT (22-KYPT-Z08).

References

[1] P. Perona, J. Malik, Scale-space and edge detection using anisotropic diffusion, IEEE Transactions on Pattern Analysis and Machine Intelligence 12(7)(1990) 629-639.

[2] L.-I. Rudin, S. Osher, E. Fatemi, Nonlinear total variation based noise removal algorithms, Physica D: Nonlinear Phenomena 60(1-4)(1992) 259-268.

[3] M.-L. Wang, X.-C. Zhou, L.-F. Zhou, L.-F. Shi, Coupling image denoising model based on total variation, Journal on Communications 37(4)(2016) 182-191.

[4] J. Yu, R. Zhai, S. Zhou, L. Tan, Image Denoising Based on Adaptive Fractional Order with Improved PM Model, Mathematical Problems in Engineering (2018) 1-11.

[5] M.-H. Zhao, Q. Wang, J. Ning, A.N. Muniru, Z. Shi, A region fusion based split Bregman method for TV Denoising algorithm, Multimedia Tools and Applications 80(10)(2021) 15875-15900.

[6] D.-L. Donoho, De-noising by soft-thresholding, IEEE Transactions on Information Theory 41(3)(1995) 612-627.

[7] X.-G. Leng, K.-F. Ji, X.-W. Xing, H. Zou, S. Zhou, Hybrid bilateral filtering algorithm based on edge detection, IET Image Process 10(11)(2016) 809-816.
[8] X.-C. Zhou, T. Wu, L.-F. Shi, M. Chen, A Kind of Wavelet Transform Image Denoising Method Based on Curvature Variation Regularization, Acta Electronica Sinica 46(3)(2018) 621-628.
[9] S. Chakraborty, S.-H. Shaikh, A. Chakrabarti, R. Ghosh, An Image Denoising Technique using Quantum Wavelet Transform, International Journal of Theoretical Physics 59(11)(2020) 3348-3371.
[10] T.O. Onur, Improved Image Denoising Using Wavelet Edge Detection Based on Otsu's Thresholding, Acta Polytechnica Hungarica 19(2)(2022) 79-92.
[11] A. Buades, B. Coll, J.-M. Morel, A non-local algorithm for image denoising, in: Proc. 2005 IEEE Computer Society Conference on Computer Vision and Pattern Recognition (CVPR'05), 2005.
[12] X.-B. Zhang, Two-step non-local means method for image denoising, Multidimensional Systems And Signal Processing 33(2)(2022) 341-366.
[13] J.-H. Zhang, Q. Zhu, J.-R. Zhang, L. Song, J.-L. Wang, A novel algorithm for threshold image denoising based on wavelet construction, Cluster Computing 22(5)(2019) 12443-12450.
[14] K. Dabov, A. Foi, V. Katkovnik, K. Egiazarian, Image denoising by sparse 3-D transform-domain collaborative filtering, IEEE Transactions on Image Processing 16(8)(2007) 2080-2095.
[15] I. Stanković, I. Djurović, M. Daković, Adaptive average BM3D filter for reconstruction of images with combined noise, in: Proc. 7th Mediterranean Conference on Embedded Computing (MECO), 2018.
[16] Q.P. Feng, S.P. Tao, C. Xu, G. Jin, BM3D-GT&AD: An Improved BM3D Denoising Algorithm Based on Gaussian Threshold and Angular Distance, IET Image Processing 14(3)(2020) 431-441.
[17] Y. Wen, Z.C. Guo, W.J. Yao, D. Yan, J.B. Sun, Hybrid BM3D and PDE filtering for non-parametric single image denoising, Signal Processing 184(2021) 108049.
[18] K. Guo, D. Labate, Optimally sparse multidimensional representation using shearlets, SIAM Journal on Mathematical Analysis 39(1)(2007) 298-318.
[19] C.-Q. Gao, P. Li, Infrared image denoising based on three-dimensional block matching, Journal of Chongqing University of Posts and Telecommunications (Nature Science Edition) 28(2)(2016) 150-155.
[20] X.-K. He, C. Wang, R.-Y. Zheng, Z.-B. Sun, X.W. Li, GPR image denoising with NSST-UNET and an improved BM3D, Digital Signal Processing 123(2022) 1-12.
[21] G. Easley, D. Labate, W.-Q. Lim, Sparse directional image representations using the discrete shearlet transform, Applied and Computational Harmonic Analysis 25(1)(2008) 25-46.
[22] S.-G. Chang, B. Yu, M. Vetterli, Adaptive wavelet thresholding for image denoising and compression, IEEE Transactions on Image Processing 9(9)(2000) 1532-1546.
[23] P. Moulin, J. Liu, Analysis of multiresolution image denoising schemes using generalized gaussian and complexity priors, IEEE Transactions on Information Theory 45(3)(1999) 909-919.
[24] M. Malfait, D. Roose, Wavelet-based image denoising using a Markov random field a priori model, IEEE Transactions on Image Processing 6(4)(1997) 549-565.